Analysis of Dynamic Thresholds for the Normalized Difference Water Index

Article *in* Photogrammetric Engineering and Remote Sensing · November 2009

DOI: 10.14358/PERS.75.11.1307

CITATIONS
877

READS
5,020

3 authors:

Lei Ji
ASRC Federal Data Solutions, Contractor to USGS Earth Resources Observation and Sc…
50 PUBLICATIONS **3,466** CITATIONS
SEE PROFILE

Li Zhang
Chinese Academy of Sciences
92 PUBLICATIONS **2,599** CITATIONS
SEE PROFILE

Bruce K. Wylie
United States Geological Survey
220 PUBLICATIONS **9,376** CITATIONS
SEE PROFILE

Analysis of Dynamic Thresholds for the Normalized Difference Water Index

Lei Ji, Li Zhang, and Bruce Wylie

Abstract

The normalized difference water index (NDWI) has been successfully used to delineate surface water features. However, two major problems have been often encountered: (a) NDWIs calculated from different band combinations [visible, near-infrared, or shortwave-infrared (SWIR)] can generate different results, and (b) NDWI thresholds vary depending on the proportions of subpixel water/non-water components. We need to evaluate all the NDWIs for determining the best performing index and to establish appropriate thresholds for clearly identifying water features. We used the spectral data obtained from a spectral library to simulate the satellite sensors Landsat ETM+, SPOT-5, ASTER, and MODIS, and calculated the simulated NDWI in different forms. We found that the NDWI calculated from (green – SWIR)/(green + SWIR), where SWIR is the shorter wavelength region (1.2 to 1.8 μm), has the most stable threshold. We recommend this NDWI be employed for mapping water, but adjustment of the threshold based on actual situations is necessary.

Introduction

The Role of Remote Sensing in Surface Water Mapping

Remote sensing techniques provide important capabilities to map surface water features and monitor the dynamics of surface water. Although active microwave sensors [e.g., the synthetic aperture radar (SAR)], are capable of penetrating darkness, clouds, and tree canopies at the longer wavelengths; they have limitations in discriminating water features from non-water covers when wind-induced waves or emergent vegetation roughen the water surface (Alsdorf e*t al.*, 2007; Smith, 1997). Passive microwave measurements can also detect water features in the presence of cloud cover and dense vegetation. But the spatial resolution is very coarse (e.g., 25 km at 37 GHZ frequency on the Special Sensor Microwave/Imager) due to the weak radiation received by the sensors (Sippel *et al.*, 1994; Smith, 1997). The data from passive visible/infrared sensors are more accessible and the interpretation of the imagery more straightforward than data from SAR imagery, although visible/infrared imagery can be affected by poor weather conditions and dense vegetation canopy. The commonly used passive visible/infrared sensors for water feature delineation include the Landsat Multispectral Scanner (MSS), Landsat Thematic Mapper (TM) and Enhanced Thematic Mapper Plus (ETM+), Advanced Very High Resolution Radiometer (AVHRR), Satellite Pour l'Observation de la Terre (SPOT), Advanced Spaceborne Thermal Emission and Reflection Radiometer (ASTER), SPOT VEGETATION, and Moderate Resolution Imaging Spectroradiometer (MODIS). Investigators have developed several different methods to map water features with the visible/infrared imagery: (a) Thematic classification method (e.g., Hung and Wu, 2005; Li, 2003; Lira, 2006), (b) Linear unmixing model (e.g., Rogers and Kearney, 2004; Sethre *et al.*, 2005), (c) single-band thresholding method (e.g., Bryant and Rainey, 2002; Jain *et al.*, 2005; Sethre *et al.*, 2005), and (d) spectral water index method (e.g., Chen *et al.*, 2004; Chipman and Lillesand, 2007; Jain *et al.*, 2006; Sakamoto *et al.*, 2007).

Use of Spectral Water Index for Delineating Water Features

The spectral water index is a single number derived from an arithmetic operation (e.g., ratio, difference, and normalized difference) of two or more spectral bands. An appropriate threshold of the index is then established to separate water bodies from other land-cover features based on the spectral characteristics. The design of a spectral water index was based on the fact that water absorbs energy at near-infrared (NIR) and shortwave-infrared (SWIR) wavelengths. The arithmetic operation not only enhances the spectral signals by contrasting the reflectance between different wavelengths, but also cancels out a large portion of the noise components that are common in different wavelength regions (i.e., sensor calibration and changing radiation conditions caused by illumination, soil, topography, and atmospheric conditions, etc.).

Adopting the format of the normalized difference vegetation index (NDVI), McFeeters (1996) developed the normalized difference water index (NDWI), defined as

$$\mathrm{NDWI} = (\rho_{\mathrm{green}} - \rho_{\mathrm{NIR}})/(\rho_{\mathrm{green}} + \rho_{\mathrm{NIR}}), \quad (1)$$

where ρ_{green} and ρ_{NIR} are the reflectance of green and NIR bands, respectively. The NDWI value ranges from −1 to 1. McFeeters (1996) set zero as the threshold. That is, the cover type is water if NDWI >0 and it is non-water if NDWI ≤0. As a side note, Gao (1996) developed a different NDWI used for

Lei Ji is with the ASRC Research and Technology Solutions, Contractor to the U.S. Geological Survey (USGS) Earth Resources Observation and Science (EROS) Center, Sioux Falls, SD 57198-0001, work performed under USGS contract 08HQCN0007 (lji@usgs.gov).

Li Zhang is with the Center for Earth Observation & Digital Earth, Chinese Academy of Sciences, P. O. Box 9718, 20A Datun Road, Chaoyang District, Beijing, 100101, P. R. China.

Bruce Wylie is with the U.S. Geological Survey, Earth Resources Observation and Science(EROS) Center, Sioux Falls, SD 57198.

Photogrammetric Engineering & Remote Sensing
Vol. 75, No. 11, November 2009, pp. 1307–1317.

0099-1112/09/7511–1307/$3.00/0

estimating water content of vegetation canopy. Although McFeeters' and Gao's NDWIs have the same terminology, the concepts of the two NDWIs are completely different. Gao's NDWI is calculated as the normalized difference of NIR and SWIR bands. Rogers and Kearney (2004) used red and SWIR bands (bands 3 and 5 in Landsat TM) to produce NDWI, given by

$$\text{NDWI} = (\rho_{\text{red}} - \rho_{\text{SWIR}})/(\rho_{\text{red}} + \rho_{\text{SWIR}}), \quad (2)$$

where ρ_{red} is the reflectance of the red band, and ρ_{SWIR} is the reflectance of the SWIR band. Xu (2006) found that McFeeters' NDWI was unable to completely separate built-up features from water features. NDWI showed positive values in built-up features which were similar to water because the NIR reflectance was lower than the green reflectance. To compensate the drawbacks of McFeeters' NDWI, Xu (2006) proposed the modified NDWI (MNDWI), in which the SWIR band (Landsat TM band 5) was used to replace the NIR band in McFeetes' NDWI equation:

$$\text{MNDWI} = (\rho_{\text{green}} - \rho_{\text{SWIR}})/(\rho_{\text{green}} + \rho_{\text{SWIR}}). \quad (3)$$

Like McFeeters' NDWI, the threshold value for MNDWI was set to zero (Xu, 2006). However, Xu (2006) found a manual adjustment of the threshold could achieve a more accurate result in the water delineation. As an independent study, Lacaux *et al.* (2007) developed a normalized difference pond index (NDPI) to classify ponds in West Africa. The NDPI is expressed as the normalized difference of green and SWIR reflectances (SPOT-5 bands 1 and 4, respectively):

$$\text{NDPI} = (\rho_{\text{SWIR}} - \rho_{\text{green}})/(\rho_{\text{SWIR}} + \rho_{\text{green}}). \quad (4)$$

The equations of MNDWI (Equation 3) and NDPI (Equation 4) are almost identical, except that the orders of ρ_{SWIR} and ρ_{green} are different in the two equations. Lacaux *et al.* (2007) used these criteria for detecting ponds: If NDPI <Threshold 1 and ρ_{SWIR} <Threshold 2, then cover is pond; otherwise, cover is not pond. Here, the two thresholds were determined for each image because the thresholds varied among different dates or sites. In the study of detecting and mapping the changes of lake shorelines, Ouma and Tateishi (2006) tested five different forms of NDWIs using Landsat TM/ETM+: $\text{NDWI}_1 = (\rho_{b7} - \rho_{b5})/(\rho_{b7} + \rho_{b5})$, $\text{NDWI}_2 = (\rho_{b4} - \rho_{b2})/(\rho_{b4} + \rho_{b2})$, $\text{NDWI}_3 = (\rho_{b5} - \rho_{b4})/(\rho_{b5} + \rho_{b4})$, $\text{NDWI}_4 = (\rho_{b5} - \rho_{b2})/(\rho_{b5} + \rho_{b2})$, and $\text{NDWI}_5 = (\rho_{b7} - \rho_{b2})/(\rho_{b7} + \rho_{b2})$, where ρ_{b2}, ρ_{b4}, ρ_{b5}, and ρ_{b7} are the reflectance of bands 2, 4, 5, and 7, respectively. In these five NDWI equations, NDWI_2 is the same as McFeeters' NDWI (Equation 1) and NDWI_4 is Xu's MNDWI (Equation 3). Ouma and Tateishi ranked the NDWIs from NDWI_1, NDWI_5, NDWI_4, NDWI_2, to NDWI_3 in order of the worst to the best performance for detecting water features. In addition to the SWIs, the NDVI derived from AVHRR has been used to map surface water bodies (e.g., Chipman and Lillesand, 2007; Ma *et al.* 2007), although the primary use of the NDVI is the detection of vegetation vigor or greenness.

Problems of Dynamic NDWI Threshold and Objectives of the Study

The NDWI data derived from Landsat MSS, TM, and ETM+ (Jain *et al.*, 2005; McFeeters, 1996; Rogers and Kearney, 2004; Ouma and Tateishi, 2006; Sethre *et al.*, 2005, Xu, 2006), SPOT (Lacaux *et al.*, 2007), MODIS (Chipman and Lillesand, 2007), AVHRR (Chipman and Lillesand, 2007; Jain *et al.*, 2006), and SPOT VEGETATION (Ma *et al.*, 2007) have been used successfully in delineating water bodies and monitoring the water area changes. In our current research on monitoring water dynamics for the wetlands in the Prairie Pothole Region, North America, and the Yukon River Basin, Alaska, we use NDWI as the primary tool to delineate the water features. However, we have found two problems that need to be understood and solved before NDWI can be appropriately used. First, the several different NDWI forms, as listed from Equation 1 to Equation 4, can generate quite different results. We need to know which NDWI among these spectral water indices performs best for delineating water features. In other words, we need to understand which band (blue, green, red, NIR, and SWIR) or band combination is the best indicator of water features. Second, the NDWI threshold is not a constant value; it is a dynamic value that changes depending on the subpixel land-cover components. An appropriate NDWI threshold needs to be determined so that the water, non-water, and mixture features can be distinguished.

Mixed pixels are caused by two or more land-cover classes in a surface area smaller than the resolution of the image. The abundance of mixed pixels in an image depends on the image resolution, land-cover heterogeneity, or details of the land-cover types in the thematic classification scheme. Mixed pixels are especially important for coarse resolution satellite images [e.g., AVHRR (1 km), SPOT VEGETATION (1 km), and MODIS (250 m)] because a large pixel usually contains multiple land-cover types within the pixel area. In land-cover classification, labeling a pixel with a class name is generally based on the criterion that the class is dominant (fraction is over 50 percent) within the pixel area. Alternatively, the criterion can be that the class is representative or important in the pixel area although the fraction of the class is lower than 50 percent. In a land surface area covered with water bodies, the image may contain pure water pixels (water fraction = 100 percent) or mixed water pixels (water fraction is a value greater than 0 percent and less than 100 percent). For water mapping, if the water class is defined as water fraction = 100 percent, the NDWI thresholds can be used in a straightforward manner. But if the water class is defined as water fraction > 50 percent, i.e., water is the dominant class in the pixel area, the NDWI is influenced by not only water but also other subordinate classes. Thus, the thresholds need to be adjusted based on the spectral signatures and proportions of the non-water components. Figure 1 illustrates three hypothetical examples of a mixed water pixel comprising 50 percent water and 50 percent non-water components. Although the water fractions are the same among the three cases shown in the examples, the fractions of non-water components are different. The reflectances and NDWIs for the three mixed pixels can also be very different due to the contrast in the spectral signatures between subpixel soil and vegetation components. Therefore, using the NDWIs to detect water features should take the influence of subpixel components on the thresholds into consideration.

In this study, we analyzed the variation of the thresholds for different NDWIs using spectral data obtained from a spectral library. Specifically, our analyses were focused on (a) the influence of soil and vegetation subpixel components on the variation of NDWI thresholds, and (b) the performance of all different forms of NDWIs based on sensitivity of the index to the subpixel components. In addition to the spectral data that simulate the satellite sensor (i.e., Landsat ETM+, SPOT-5, ASTER, and MODIS), we also used the real satellite images to demonstrate the procedure of surface water mapping using NDWI.

Data and Methods

Our analysis focused on the spectral characteristics of water, soil, and vegetation because these three components constitute major land-cover types on land surfaces. We used a hyperspectral data set to simulate the spectral bands of Landsat ETM+, SPOT, ASTER, and MODIS for each of these three land-cover components. The hyperspectral data were obtained from the ASTER Spectral Library (California Institute of Technology

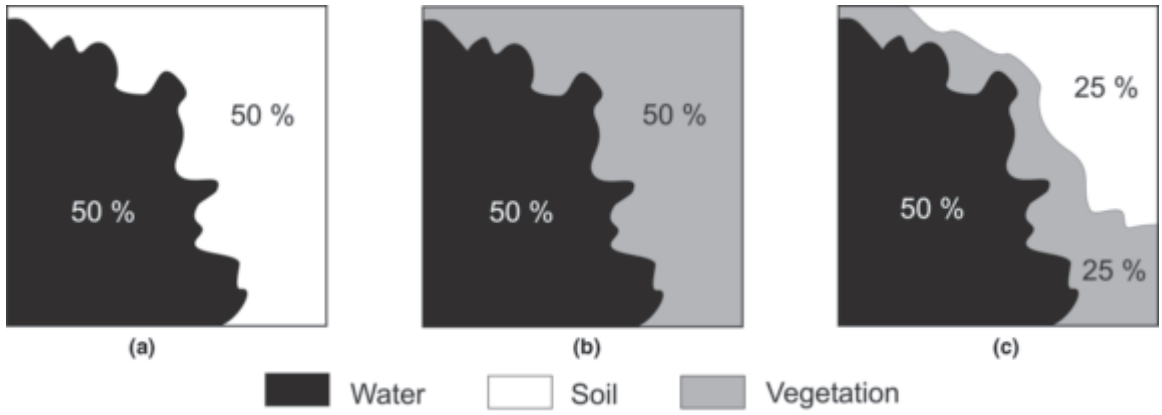

Figure 1. Hypothetical examples of mixed water pixels comprising 50 percent water and 50 percent non-water components. The square represents a single pixel in an image, and the water, soil, and vegetation are the subpixel components: (a) Water fraction = 50%; soil fraction = 50%, (b) Water fraction = 50%; vegetation fraction = 50%, and (c) Water fraction = 50%; soil fraction = 25%; vegetation fraction = 25%.

Jet Propulsion Laboratory, 2008). We selected Tap Water, Grayish Brown Loam, and Green Rye Grass from the spectral library to represent the water, soil, and vegetation classes, respectively. The visible to SWIR spectrum (0.4 to 2.5 μm) for these samples was recorded using a Beckman IUV 5240 spectrophotometer at Johns Hopkins University IR-spectroscopy. The spectral interval is 0.001 μm in the region from 0.4 to 0.8 μm, and 0.004 μm from 0.8 to 2.5 μm.

Figure 2 demonstrates the spectral reflectances of the water, soil, and vegetation samples obtained from the spectral library. To simulate the Landsat ETM+, SPOT-5, ASTER, and MODIS sensors, we calculated the mean value of the spectral reflectance for each sensor band. Figure 3 shows the reflectances of water, soil, and vegetation simulated to the six Landsat ETM+ bands, four SPOT-5 bands, nine ASTER bands, and seven MODIS bands from the visible to SWIR region. We

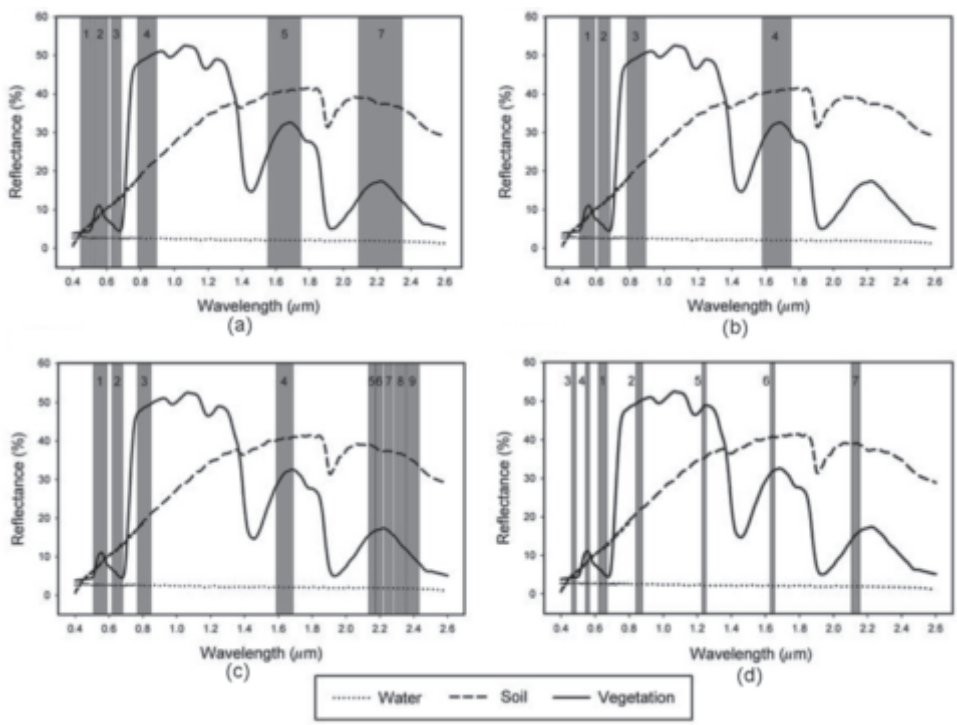

Figure 2. Spectra of water, soil, and vegetation samples. The spectral bands of (a) Landsat ETM+, (b) SPOT-5, (c) ASTER, and (d) MODIS are represented by the vertical gray bars with the numbers indicating the band names. The spectral data are derived from the California Institute of Technology Jet Propulsion Laboratory (2008).

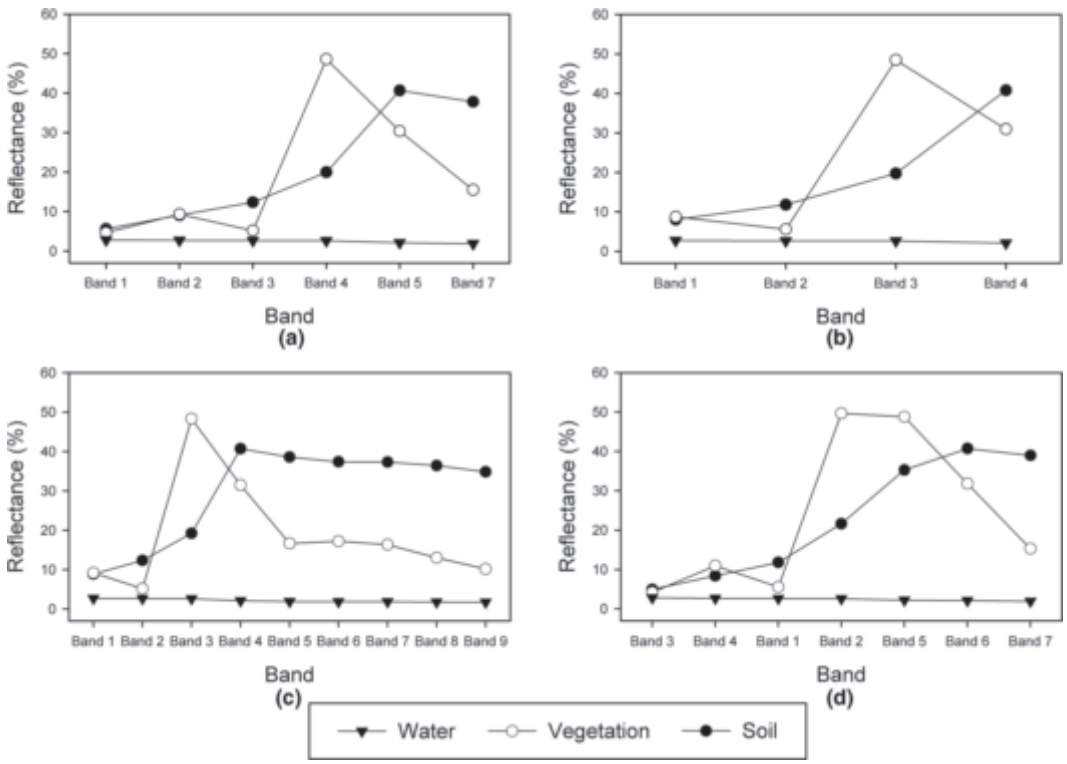

Figure 3. Reflectance of water, soil, and vegetation samples simulated to the (a) Landsat ETM+, (b) SPOT-5, (c) ASTER, and (d) MODIS bands. The reflectance for each band is the mean value of the spectral reflectance of water, soil, or vegetation sample over the range of the band wavelength. The three samples obtained from the spectral library are treated as endmembers of water, soil, and vegetation to simulate the mixed spectral signatures.

treated the water, soil, and vegetation samples as three endmembers, and then we simulated the mixed spectral signatures using the endmember signatures. An endmember is the pure component of water, soil, or vegetation, representing a pure pixel in an image. A mixture of the two or three endmembers represents a mixed pixel consisting of mixed spectral signatures of the three components. We analyzed the mixture of spectral signatures based on the linear mixture model theory. The assumption of the linear mixture model is that the different components in a pixel contribute independently to its reflectance. Therefore, the reflectance of a pixel at a particular band is the sum of the reflectances of all subpixel components at that band. For our specific case, the reflectance of water, soil, and vegetation mixture is the sum of the reflectances of the three individual components:

$$\rho_i = \rho_{w,i} f_w + \rho_{s,i} f_s + \rho_{v,i} f_v, \quad (f_w + f_s + f_v = 100\%) \qquad (5)$$

where ρ_i is the reflectance of mixed water, soil, and vegetation in spectral band i; $\rho_{w,i}$, $\rho_{s,i}$, and $\rho_{v,i}$, respectively, are the reflectances of pure water, soil, and vegetation in band i; f_w, f_s, and f_v are the fractions (percent) of water, soil, and vegetation, respectively.

To simulate the reflectances of the water, soil, and vegetation mixtures, we used various proportions of the three components. The fraction of each component ranges from 0 percent to 100 percent with an increment of 5 percent (the sum of the fractions of the three components is 100 percent). The reflectances of the mixtures were calculated following Equation 5. The ternary diagram shown in Figure 4 illustrates all possible fractions of each component in a water, soil, and vegetation mixture. In the diagram, each intersection of three lines represents a mixture with three different fractions of water, soil, and vegetation. For example, Point A in the diagram represents a mixture of $f_w = 75\%$, $f_s = 20\%$, and $f_v = 5\%$; Point B is a mixture of $f_w = 40\%$, $f_s = 0\%$, and $f_v = 60\%$. In the simulation, we calculated the reflectances of multiple bands for 231 mixtures, corresponding to 231 intersections in the ternary diagram (Figure 4). The reflectances of the simulated Landsat ETM+, SPOT-5, ASTER, and MODIS bands are then used to calculate NDWI. With different band combinations, we obtained 2 to 4 different NDWI equations for each sensor as shown in Table 1. Because ASTER bands 5, 6, 7, 8, and 9 in the SWIR region are all very similar, we only calculated the NDWI for band 7 as a representative, which is located at the center of the five SWIR bands.

We have noted that the general formula of the NDWI, regardless of sensors, is expressed as the normalized difference between the green band and the NIR (or SWIR) band. The reason for using the green band instead of the red band is that soil and vegetation have a similar reflectance in the green band (Figures 2 and 3). However, vegetation has a much lower reflectance in the red band than soil due to the chlorophyll absorption in green vegetation. Therefore, the green band is relatively insensitive to the background components. In this paper, McFeeters' NDWI (Equation 1) is expressed as $NDWI_{L2,4}$, which is similar to the $NDWI_{S1,3}$, $NDWI_{A1,3}$, and $NDWI_{M4,2}$ of other sensors (Table 1). Xu's MNDWI (Equation 3) is known as $NDWI_{L2,5}$, which is similar to $NDWI_{S1,4}$, $NDWI_{A1,4}$, $NDWI_{M4,5}$, and $NDWI_{M4,6}$ (Table 1).

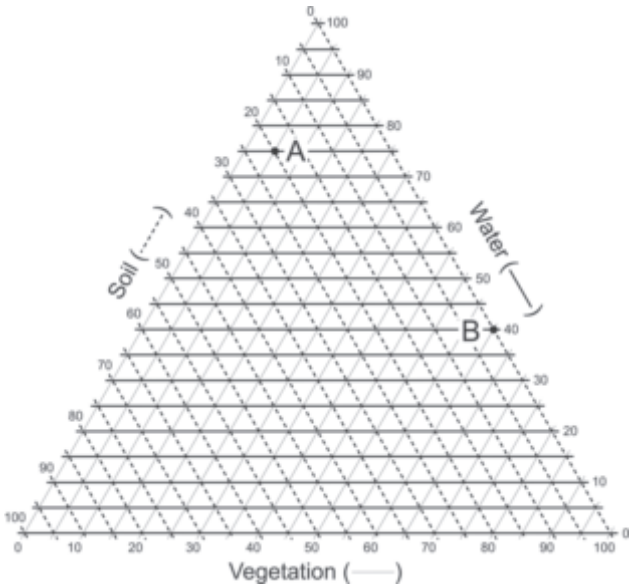

Figure 4. Ternary diagram for water, soil, and vegetation mixtures. Each intersection of three lines represents a mixture consisting of three different fractions of water (thick solid line), soil (dashed line), and vegetation (thin solid line). For example, Point A represents a mixture of f_w = 75%, f_s = 20%, and f_v = 5%; Point B is a mixture of f_w = 40%, f_s = 0%, and f_v = 60%.

Results and Discussion

Influence of Mixed Components on the NDWI Thresholds

The influence of the three mixed components (water, soil, and vegetation) on the NDWI values is illustrated in Figures 5 and 6. As described previously, we calculated the NDWI values for 231 different mixtures. Each mixture consists of any of the three components ranging from 0 percent to 100 percent with an increment of 5 percent. In the graphs shown in Figures 5 and 6, the NDWI values are plotted against the soil and vegetation fractions for each level of water fraction (f_w = 0%, 10%, ... 100%). For a comparison, NDVI values are also plotted on the same graphs, which is useful to indicate the relative proportions of soil and vegetation. Figure 5 shows the NDWI values simulated for the Landsat ETM+ sensor, including $NDWI_{L2,4}$, $NDWI_{L2,5}$, and $NDWI_{L2,7}$. The NDWI values simulated for the MODIS sensor, i.e., $NDWI_{M4,2}$, $NDWI_{M4,5}$, $NDWI_{M4,6}$, and $NDWI_{M4,7}$, are demonstrated in Figure 6. Plots of SPOT-5 and ASTER data are not presented in the paper due to the limit of the paper length.

According to the analysis shown in Figures 5 and 6, when water fraction is 100 percent, the thresholds of NDWIs have their unique values (Table 2). That is, if we assume that a target is pure water, the NDWI value is capable of distinguishing water from non-water based on the threshold. However, when the target is a mixture, i.e., when water fraction is less than 100 percent, the NDWI values are substantially lower than the case of pure water (Table 2). Therefore, in water mapping, if the water class is defined as f_w = 100%, using the unique thresholds is appropriate. But if the definition of the water class is a different water fraction (e.g., f_w = 50% or f_w = 75%), the thresholds need to be lowered. Moreover, for a given water fraction, the thresholds vary considerably depending on the fractional components of soil and vegetation. For example (Table 2), given f_w = 50%, if f_s = 0% and f_v = 50%, the simulated MODIS NDWI thresholds are $NDWI_{M4,2} = -0.585$, $NDWI_{M4,5} = -0.577$, $NDWI_{M4,6} = -0.425$, and $NDWI_{M4,7} = -0.116$. But if f_s = 50% and f_v = 0%, the NDWI thresholds are $NDWI_{M4,2} = -0.372$, $NDWI_{M4,5} = -0.543$, $NDWI_{M4,6} = -0.588$, and $NDWI_{M4,7} = -0.573$. As a result, the fractional components of soil and vegetation have a strong impact on the NDWI values. In any case, when the water class is defined as f_w = 50% or other fractions, the NDWI thresholds need to be adjusted according to relative proportions of the soil and vegetation components.

Performance of Different NDWIs for Water Delineation

When f_w <100%, the NDWI values show significant variations, which depend on the relative fractions of soil and vegetation, as demonstrated in Figures 5 and 6. For the simulated Landsat ETM+ sensor, $NDWI_{L2,5}$, $NDWI_{L2,7}$, and NDVI increase with the vegetation fraction, while $NDWI_{L2,4}$ decreases with the vegetation fraction. For the MODIS sensor, as the vegetation fraction increases, $NDWI_{M4,6}$, $NDWI_{M4,7}$, and NDVI increase, but $NDWI_{M4,2}$ decreases. $NDWI_{M4,5}$ stays

TABLE 1. NDWI EQUATIONS AND ASSOCIATED SENSORS AND BANDS

Sensor	NDWI equation	Symbol and notation	Band wavelength (μm)
Landsat ETM+	$NDWI_{L2,4} = (\rho_{L2} - \rho_{L4})/(\rho_{L2} + \rho_{L4})$ $NDWI_{L2,5} = (\rho_{L2} - \rho_{L5})/(\rho_{L2} + \rho_{L5})$ $NDWI_{L2,7} = (\rho_{L2} - \rho_{L7})/(\rho_{L2} + \rho_{L7})$	$NDWI_{L2,4}$, $NDWI_{L2,5}$, and $NDWI_{L2,7}$ are the NDWI values of bands 2, 4, 5, and 7; ρ_{L2}, ρ_{L4}, ρ_{L5}, and ρ_{L7} are the reflectances of bands 2, 4, 5, and 7	Band 2 (green): 0.52 − 0.60 Band 4 (NIR): 0.77 − 0.90 Band 5 (SWIR): 1.55 − 1.75 Band 7 (SWIR): 2.09 − 2.35
SPOT-5	$NDWI_{S1,3} = (\rho_{S1} - \rho_{S3})/(\rho_{S1} + \rho_{S3})$ $NDWI_{S1,4} = (\rho_{S1} - \rho_{S4})/(\rho_{S1} + \rho_{S4})$	$NDWI_{S1,3}$ and $NDWI_{S1,4}$ are the NDWI values of bands 1, 3, and 4; ρ_{S1}, ρ_{S3}, and ρ_{S4} are the reflectances of bands 1, 3, and 4	Band 1 (green): 0.50 − 0.59 Band 3 (NIR): 0.78 − 0.89 Band 4 (SWIR): 1.58 − 1.75
ASTER	$NDWI_{A1,3} = (\rho_{A1} - \rho_{A3})/(\rho_{A1} + \rho_{A3})$ $NDWI_{A1,4} = (\rho_{A1} - \rho_{A4})/(\rho_{A1} + \rho_{A4})$ $NDWI_{A1,7} = (\rho_{A1} - \rho_{A7})/(\rho_{A1} + \rho_{A7})$	$NDWI_{A1,3}$, $NDWI_{A1,4}$, and $NDWI_{A1,7}$ are the NDWI values of bands 1, 3, 4, and band 7; ρ_{A1}, ρ_{A3}, ρ_{A4}, and ρ_{A7} are the reflectances of bands 1, 3, 4, and 7.	Band 1 (green): 0.52 − 0.60 Band 3 (NIR): 0.78 − 0.86 Band 4 (SWIR): 1.60 − 1.70 Band 7 (SWIR): 2.24 − 2.29
MODIS	$NDWI_{M4,2} = (\rho_{M4} - \rho_{M2})/(\rho_{M4} + \rho_{M2})$ $NDWI_{M4,5} = (\rho_{M4} - \rho_{M5})/(\rho_{M4} + \rho_{M5})$ $NDWI_{M4,6} = (\rho_{M4} - \rho_{M6})/(\rho_{M4} + \rho_{M6})$ $NDWI_{M4,7} = (\rho_{M4} - \rho_{M7})/(\rho_{M4} + \rho_{M7})$	$NDWI_{M4,2}$, $NDWI_{M4,5}$, $NDWI_{M4,6}$, and $NDWI_{M4,7}$ are the NDWI values of bands 4, 2, 5, 6, and 7; ρ_{M4}, ρ_{M2}, ρ_{M5}, ρ_{M6}, and ρ_{L7} are the reflectance of bands 4, 2, 5, 6, and 7	Band 4 (green): 0.55 − 0.57 Band 2 (NIR): 0.84 − 0.88 Band 5 (SWIR): 1.23 − 1.25 Band 6 (SWIR): 1.63 − 1.65 Band 7 (SWIR): 2.11 − 2.16

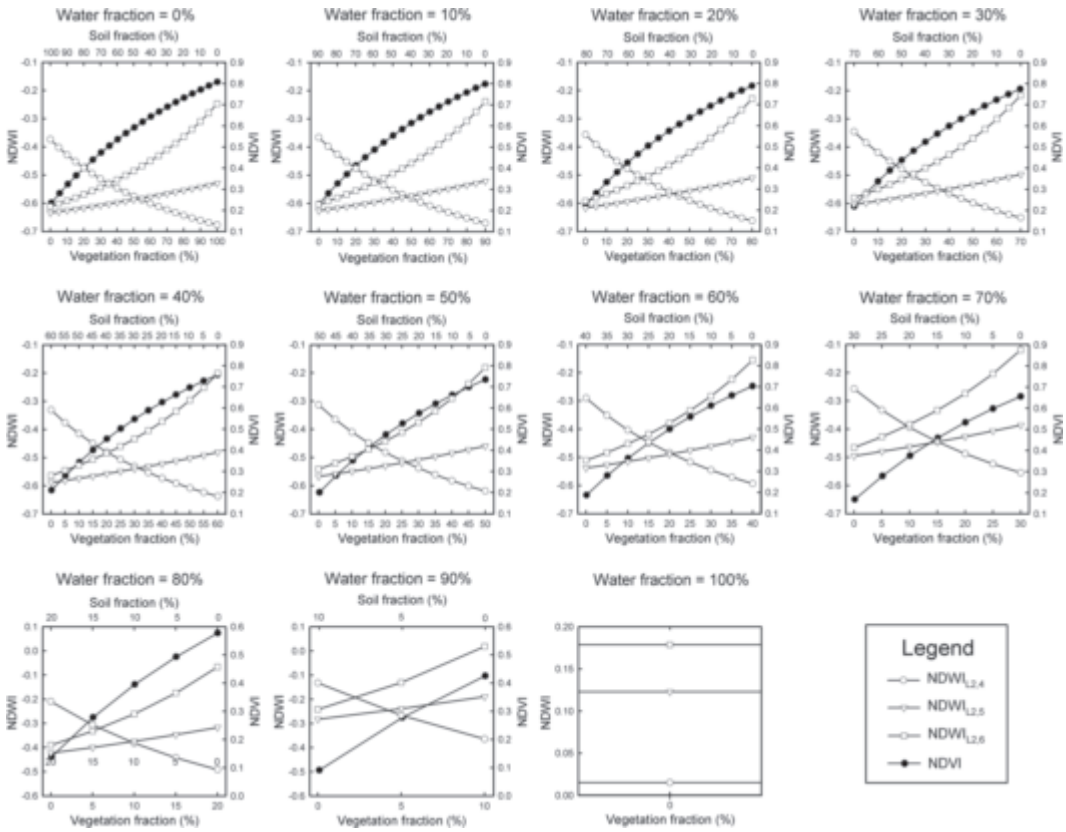

Figure 5. Variation of the Landsat-simulated NDWI values for the mixtures with different fractions of water, soil, and vegetation components. For a given water fraction (>0), the NDWI thresholds are the functions of the fractions of soil and vegetation. The NDVI is used to indicate the relative proportion between soil and vegetation.

relatively constant because NIR reflectance (ETM+ band 4; MODIS band 2) is positively proportional to the amount of vegetation, while SWIR reflectances (ETM+ bands 5 and 7; MODIS bands 6 and 7) have negative relationships to the amount of vegetation (Figure 3). As a result, the mixture containing more vegetation will have higher NIR reflectance and lower SWIR reflectance. Thus, the mixture of more vegetation simulated for the Landsat ETM+ will have higher $NDWI_{L2,5}$, $NDWI_{L2,7}$, and NDVI and lower $NDWI_{L2,4}$. Similarly, for this mixture simulated for MODIS, we can observe higher $NDWI_{M4,6}$, $NDWI_{M4,7}$, and NDVI and lower $NDWI_{M4,2}$ and $NDWI_{M4,5}$.

From Figures 5 and 6, we note that for a given water fraction (f_w = 0%, 5%, . . . , 95%), each NDWI or NDVI has varying values depending on the fractional components of soil and vegetation. The variations, however, differ greatly among the different NDWIs or NDVI. For example, for the simulated MODIS indices when f_w = 50%, $NDWI_{M4,7}$ changes from −0.573 to −0.116 with a range of 0.407, while $NDWI_{M4,5}$ has only a small range (0.034), changing from −0.543 to −0.577. Now we can compare all NDWIs and NDVI with regard to their variations for every interval of water fraction. The variation of NDWI and NDVI is represented by the range of the index, i.e., the difference between the maximum and minimum values for the index. Figure 7 demonstrates the ranges of all NDWIs and NDVI for the simulated Landsat ETM+, SPOT-5, ASTER, and MODIS sensors. The range of the NDWI or NDVI indicates the sensitivity of the index to the non-water components. Generally, the indices with lower ranges are less sensitive to the fractional components of soil and vegetation. We notice that for the four satellite sensors, the NDWIs calculated from the green and SWIR (1.2 to 1.8 μm region) bands have relatively low ranges. Among them, $NDWI_{M4,5}$ has the lowest range values. Thus, these are the best NDWIs, which are relatively independent of the soil and vegetation components. The next low NDWI ranges are the NDWI calculated from the green and NIR bands. The NDWIs based on green and SWIR (>2.0 μm) have the highest ranges. They are not recommended because of the large variations caused by the soil and vegetation background. NDVI, in all the four sensors, has the greatest range and thus the strongest sensitivity to the soil and vegetation.

Inspecting the spectral signals of soil and vegetation in the NIR and SWIR wavelengths as shown in Figures 2 and 3, we notice that the soil and vegetation have the smallest difference in the shorter SWIR (1.2 to 1.8 μm) reflectance. But the reflectances of soil and vegetation differ considerably in the NIR band and the longer region (>2.0 μm) of the SWIR band. This implies that the shorter SWIR band is less sensitive to the change of soil and vegetation components than the NIR band or the longer SWIR band. These phenomena explain why the NDWI calculated from the shorter SWIR band has the smallest NDWI range while the range of the NDWI calculated from the NIR band or longer SWIR band is much bigger.

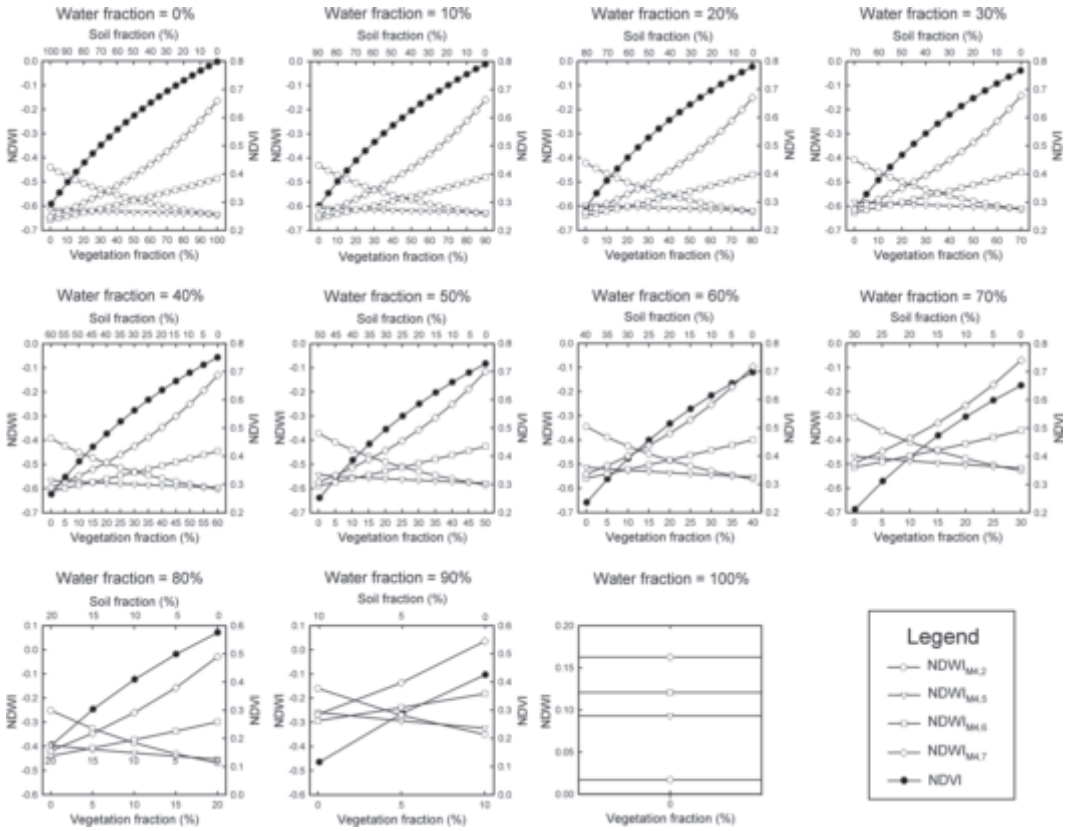

Figure 6. Variation of the MODIS-simulated NDWI values for the mixtures with different fractions of water, soil, and vegetation components. For a given water fraction (>0), the NDWI thresholds are the functions of the fractions of soil and vegetation. The NDVI is used to indicate the relative proportions of soil and vegetation.

Procedure of Delineating Surface Water with NDWI

We recommend an eight-step general procedure for using the satellite-derived NDWI to delineate surface water features:

1. Decide which satellite data sets are most appropriate for specific applications to map land surface water. The important considerations for selecting satellite data sets are spatial coverage, spatial resolution, temporal resolution, and band characteristics. The specific objectives and requirements of a water mapping project dictate appropriate satellite data sources.
2. Decide what data sets are used as the reference data. The reference data sets are used to (a) adjust or calibrate the NDWI threshold for the mapping data set, and (b) assess the accuracy of the water mapping results. The reference data sets can be some small image subsets in space, but they should be accurate with respect to water delineation or relatively accurate compared with the mapping data. In general, finer resolution images can be used as reference data if coarser resolution images are used for mapping surface water features. For example, Landsat TM/ETM+ (30 m), SPOT (20 m), or ASTER (15 m for visible and NIR band and 30 for SWIR band) images can be used as reference data if the mapping data are the 500 m MODIS products. But, if Landsat images are used in water mapping, good reference data are fine resolution satellite images such as Ikonos (4 m) and QuickBird (2.4 m), aerial photographs, or even ground observations.
3. Define the water classes based on the fractional water component in the image. For the high-resolution images, we can use only one water class, which is defined as $f_w \geq 50\%$. The output image is a two-class map: water ($f_w \geq 50\%$) and non-water ($f_w < 50\%$). But if we use coarse resolution images (e.g., AVHRR or MODIS) to map water bodies, we may have two or more water classes, for example, water ($f_w => 75\%$) and water-land mixture (f_w = 25 to 75%).
4. Select an NDWI from all different NDWIs based on the performance analysis of these indices. In this study, we have demonstrated that $NDWI_{L2,5}$, $NDWI_{S1,4}$, $NDWI_{A1,4}$, and $NDWI_{M4,5}$ are the best indices for delineating surface water in Landsat ETM+, SPOT, ASTER, and MODIS, respectively, because they are least sensitive to the subpixel non-water components. In general, an NDWI that uses green and SWIR bands (<1.8 μm) is the best index for delineating water features.
5. Use the NDWI thresholds to density-slice the image to generate initial water classes as defined in Step 3. We have noticed that the thresholds are different depending on different definitions of water classes. When the definition of the water class is $f_w = 100\%$, using the NDWI thresholds is straightforward (Table 2). If the water class is defined as $f_w < 100\%$ (e.g., f_w = 25%, 50%, or 75%), we need to use the threshold that corresponds to the water fraction. However, for a given water fraction ($f_w < 100\%$), the NDWI threshold can be different with the change of the fractional soil and vegetation components. To simplify the complexity, we can assume the soil and vegetation fractions are equal (i.e., $f_s = f_v$) for a given water fraction and use the NDWI threshold when $f_s = f_v$. For an example of water mapping using $NDWI_{M4,5}$, if the class water-land mixture (f_w = 25 − 75%) is to be determined, we can use $NDWI_{M4,5} = -0.603$ for f_w = 25% and $f_s = f_v$ = 37.5%, and $NDWI_{M4,5} = -0.466$ for f_w = 75% and $f_s = f_v$ = 12.5%. In fact, $NDWI_{M4,5}$ is fairly invariable within the range of the soil and vegetation fractions. We have found that although the

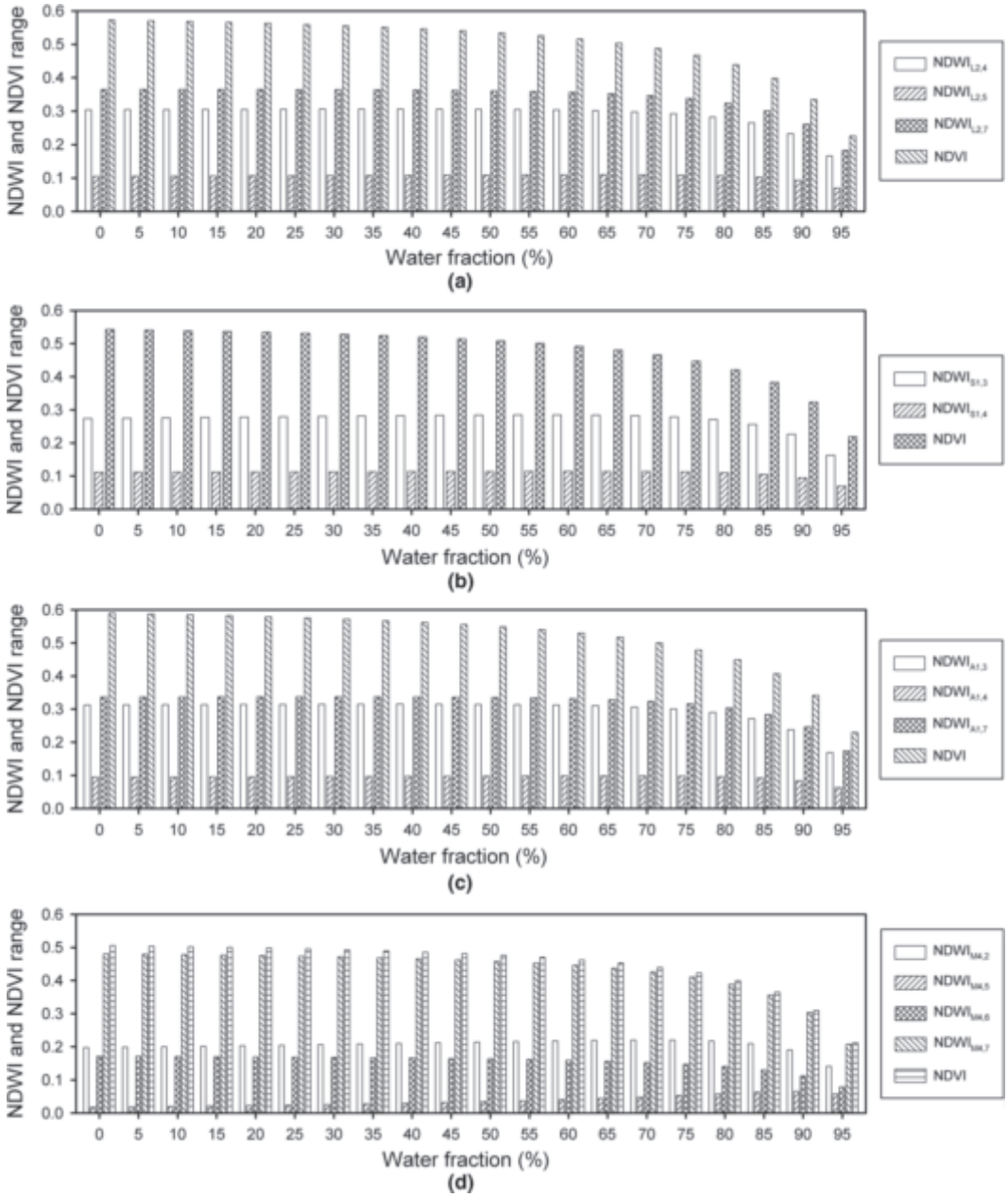

Figure 7. Comparison of the ranges of NDWIs and NDVI for different water fractions: (a) Landsat EMT+, (b) SPOT-5, (c) ASTER, and (d) MODIS. The ranges of NDWIs and NDVI are calculated by the difference between the maximum and minimum values for a given water fraction. The higher ranges indicate that the index is more sensitive to the relative proportions of the soil and vegetation components.

NDWI threshold indicated in Table 2 can be used to determine the initial NDWI threshold, examining the histogram of the NDWI image can help to locate the threshold more efficiently.

6. Compare the initial water map with the reference data as described in Step 2, and then adjust the NDWI threshold if the initial water map is overestimated or underestimated. The NDWI threshold needs to be continuously adjusted until the water map agrees well with the reference data.
7. Some bright targets on images like rocks, sand, snow, ice, and built-ups usually have high negative NDWI values, which may be confused with water features. Because these cover features unexceptionally have high reflectance in SWIR, we can use an additional threshold in the SWIR band to separate the water features from these bright cover types.
8. Assess the mapping accuracy by comparing the water mapping products with the independent reference data sets.

We now demonstrate the samples of mapping surface water using the Landsat TM and MODIS images for the lakes in eastern South Dakota. The lakes for water mapping are mainly Dry Lake, Lake Poinsett, Lake Albert, Lake St John, Lake Norden, and Lake March located in Hamlin, Brookings, and Kingsbury Counties (Plate 1). The 30 m resolution Landsat TM image used is a scene of path 29/row 29

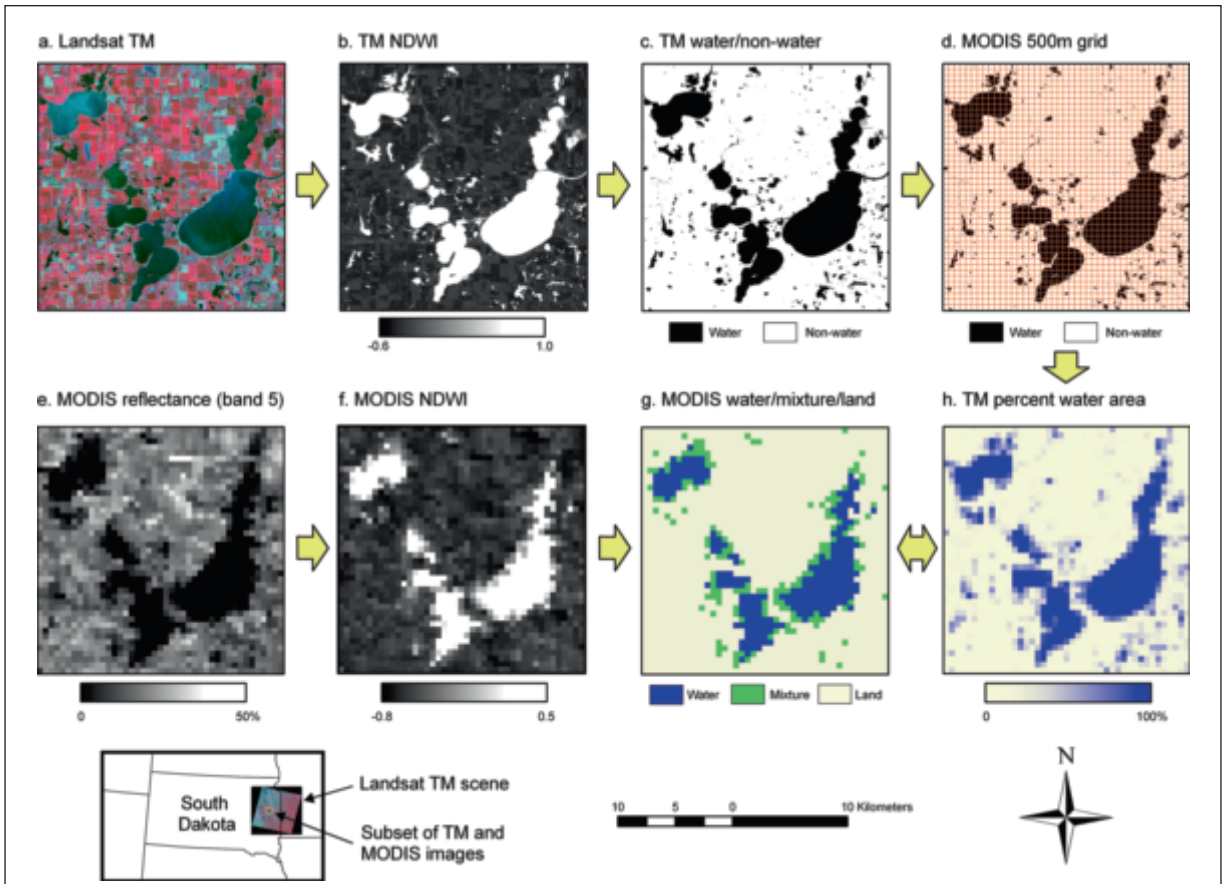

Plate 1. Examples of mapping surface water features in eastern South Dakota using Landsat TM and MODIS images. The extent of the images shown as examples is indicated as a yellow box in the location map on the bottom: (a) Subset of Landsat TM image, path/row 29/29, 04 August 2001, false-color composite (RGB = 432), (b) NDWI calculated from TM bands 2 and 5, (c) Water/non-water binary map derived from the TM NDWI image, (d) MODIS 500 m by 500 m grid overlaying on the TM water/non-water map, (e) eight-day composite (28 July to 04 August 2001) MODIS surface reflectance image (band 5), (f) MODIS NDWI calculated based on bands 4 and 5, (g) Map of water, water-land mixture, and land derived by thresholding MODIS NDWI, and (h) Map of percent water area derived from TM binary water/non-water map.

observed on 04 August 2001. The image was acquired from the Multi-Resolution Land Characterization (2001) At-Sensor Reflectance Dataset (**http://www.mrlc.gov/**), in which the original digital number has been converted to the at-sensor reflectance (Plate 1a). As suggested previously, $NDWI_{L2,5}$ was calculated (Table 1, Plate 1b) and the $NDWI_{L2,5}$ image used to delineate surface water features. In this case, the output map has two classes, water ($f_w \geq 50\%$) and non-water ($f_w < 50\%$). We initially set the Landsat $NDWI_{L2,5}$ threshold to -0.52 according to the spectral library data (Table 2). At this step, the "initial" threshold is not determinate because of the difference between the laboratory-based and the satellite-based spectra: the laboratory data do not account for the atmospheric effect while atmospheric correction algorithms have partially applied to the Landsat at-sensor reflectance images. The initial water/non-water map was compared with the TM false-color composite image; then the $NDWI_{L2,5}$ threshold was manually adjusted to reach the best agreement. We found that when $NDWI_{L2,5} = -0.20$, the binary output water map (Plate 1c) agrees best with the false-color image. We should mention that a better mapping result would be achieved if the Landsat NDWI thresholds could be quantitatively adjusted and validated using finer resolution satellite images (e.g., Ikonos and QuickBird) or aerial photographs observed on the same day or close enough.

In the example of water mapping with coarse resolution imagery, we used the 500 m, eight-day composite (28 July to 04 August 2001) MODIS Terra reflectance data (MOD09A1, version 4, **http://lpdaac.usgs.gov/dataproducts.asp**) to map the lakes in east South Dakota as described above (Plate 1e). Although the resolution is coarse, the MODIS data set has the advantages of very large coverage and frequent observations compared to finer resolution satellite data such as Landsat and SPOT. Use of MODIS data is suitable for temporally monitoring surface water dynamics at a large scale. Because the resolution is coarse, we decided to classify the land-covers into three categories: water ($f_w > 75\%$), water-land mixture ($f_w = 25$ to 75%), and land ($f_w < 25\%$). We computed the $NDWI_{M4,5}$ image (Plate 1f) and determined that the two $NDWI_{M4,5}$ thresholds were initially set to -0.603 and -0.466 based on the spectral data analysis (Table 2). We did not use the 250 m MODIS reflectance data in this study, although the resolution of the product is finer. It is impossible to compare the performances of the different NDWI formulas with the 250 m MODIS data because the green and SWIR bands are not available in this product.

In this case, the Landsat TM-derived water/non-water binary map (Plate 1c), which has a relatively fine resolution, can be used as a reference data set to calibrate the MODIS NDWI. The 30 m resolution TM-derived map, however, needed to be aggregated to 500 m resolution to match the MODIS image resolution. For this purpose, we generated a 500 m by 500 m grid coverage that matches the MODIS pixels (Plate 1d). The numbers of 30 m water and non-water pixels within each 500 m by 500 m grid were counted and then converted to percent values. The output of the percent values was the map of the TM-derived percent water area at 500 m resolution (Plate 1h), which was used for calibrating the MODIS NDWI thresholds. The map of percent water area was then compared with the initial map of MODIS water/mixture/land derived from $NDWI_{M4,5}$. By adjusting the $NDWI_{M4,5}$ thresholds, we were able to produce the final map of the MODIS-derived water/mixture/land classes that best match the TM-derived percent water map. The final $NDWI_{M4,5}$ thresholds are -0.510 for separating water and water-land mixture and -0.300 for separating water-land mixture and land.

We have introduced an NDWI thresholding method for delineating surface water features and provided real examples of surface water mapping with the Landsat TM and the MODIS data. Because the NDWI thresholds analyzed in this paper is based solely on laboratory data, the thresholds are not adequate to apply directly to satellite images in reality. The thresholds, however, can be used as initial values and then be calibrated using the reference data. Some problems that are not considered in the spectral library data may exist in satellite data that are used to derive the NDWI. Therefore, adjustment of the NDWI threshold is critical in the applications of water mapping with satellite data. The major factors that may cause the difference between laboratory data and satellite data are listed below:

1. Complexity of land-covers in the real world. The spectral library data used in this study were based on the spectral measurement of three pure materials. The land-cover types in the real world are usually more diverse and complicated, which would affect the variations in the spectral signals and hence NDWI values. For natural water bodies, the physical, chemical, and biological substances containing in water (e.g., suspended sediments, algal chlorophyll, and aquatic vegetation) can also cause the deviation in the spectra from the pure water.
2. Atmospheric effect on satellite images as discussed previously. Even though for the satellite data corrected for the atmospheric effect, the correction would not be perfect.
3. Seasonality of satellite data time series. The seasonal influence includes not only the seasonal variations in atmospheric conditions, but also the seasonal changes in land surface conditions (e.g., vegetation greenness, vegetation moisture and soil moisture). Seasonality is especially important for vegetation, which changes greatly from the early and middle (greening) to the late (senescence) growing season.
4. Impact of shadows (e.g., mountain, tree, or building shadow) on satellite images, especially high-resolution images.

Conclusions

In this study, we simulated spectral reflectances for all visible, NIR, and SWIR bands of four satellite sensors, i.e., Landsat ETM+, SPOT, ASTER, and MODIS, using spectral library data sets. We treated the spectra of water, soil, and vegetation from the spectral library as endmembers and then simulated the mixed spectral signatures using the endmember signatures. We calculated different forms of the NDWIs based on simulated green, NIR, and SWIR bands for pure water, soil, and vegetation component and various mixtures of these components. The simulated NDWI threshold values were found to be influenced by the fractions of soil and vegetation at a given water fraction (>0%). It was also discovered that the NDWI calculated from (green − SWIR)/(green + SWIR), where the SWIR band is in the region of shorter wavelength (1.2 to 1.8 μm), has the most stable threshold. Specifically for the four satellite sensors mentioned above, we recommend $NDWI_{L2,5}$, $NDWI_{S1,4}$, and $NDWI_{A1,4}$, $NDWI_{M4,5}$ for use in mapping surface water features because these four indices have the least impact from subpixel vegetation component. Additionally, we found NDVI is very sensitive to the subpixel vegetation component; therefore, NDVI is not suitable for delineating

TABLE 2. NDWI AND NDVI THRESHOLDS FOR PURE WATER (F_w = 100%) AND MIXED WATER (F_w = 25%, 50%, AND 75%) COMPONENTS

		NDWI and NDVI threshold									
		f_w = 25%			f_w = 50%			f_w = 75%			f_w = 100%
Sensor	Spectral water index	f_s = 75% f_v = 0%	f_s = 37.5% f_v = 37.5%	f_s = 0% f_v = 75%	f_s = 50% f_v = 0%	f_s = 25% f_v = 25%	f_s = 0% f_v = 50%	f_s = 25% f_v = 0%	f_s = 12.5% f_v = 12.5%	f_s = 0% f_v = 25%	f_s = 0% f_v = 0%
Landsat ETM+	$NDWI_{L2,4}$	−0.351	−0.553	−0.657	−0.313	−0.512	−0.619	−0.236	−0.416	−0.528	0.015
	$NDWI_{L2,5}$	−0.611	−0.563	−0.504	−0.568	−0.519	−0.459	−0.464	−0.414	−0.356	0.123
	$NDWI_{L2,7}$	−0.587	−0.458	−0.223	−0.542	−0.410	−0.181	−0.433	−0.300	−0.096	0.179
	NDVI	0.223	0.569	0.782	0.201	0.527	0.735	0.156	0.430	0.622	−0.007
SPOT-5	$NDWI_{S1,3}$	−0.394	−0.595	−0.672	−0.350	−0.535	−0.633	−0.261	−0.433	−0.539	0.016
	$NDWI_{S1,4}$	−0.645	−0.587	−0.532	−0.599	−0.547	−0.485	−0.488	−0.437	−0.376	0.124
	NDVI	0.237	0.601	0.767	0.213	0.527	0.721	0.164	0.429	0.611	−0.008
ASTER	$NDWI_{A1,3}$	−0.345	−0.554	−0.659	−0.307	−0.512	−0.621	−0.229	−0.415	−0.529	0.015
	$NDWI_{A1,4}$	−0.618	−0.574	−0.522	−0.574	−0.530	−0.477	−0.469	−0.424	−0.372	0.124
	$NDWI_{A1,5}$	−0.590	−0.468	−0.253	−0.544	−0.419	−0.209	−0.433	−0.307	−0.117	0.186
	NDVI	0.206	0.564	0.781	0.186	0.522	0.734	0.143	0.425	0.621	−0.007
MODIS	$NDWI_{M4,2}$	−0.415	−0.550	−0.619	−0.372	−0.511	−0.585	−0.282	−0.418	−0.502	0.017
	$NDWI_{M4,5}$	−0.590	−0.603	−0.613	−0.543	−0.563	−0.577	−0.436	−0.466	−0.489	0.093
	$NDWI_{M4,6}$	−0.633	−0.555	−0.465	−0.588	−0.512	−0.425	−0.481	−0.411	−0.334	0.121
	$NDWI_{M4,7}$	−0.620	−0.448	−0.147	−0.573	−0.403	−0.116	−0.462	−0.298	−0.052	0.163
	NDVI	0.278	0.584	0.773	0.252	0.542	0.728	0.196	0.444	0.619	−0.009

water unless the SWIR bands are not available in the sensor. In the applications of mapping surface water bodies using the NDWI method, the NDWI threshold should be adjusted to match a reference data set that has a finer spatial resolution.

Acknowledgments

This research was funded by the USGS through the Earth Surface Dynamics program, the Climate Effects Network, and the Land Remote Sensing and Geographic Analysis and Monitoring programs. The spectral library data presented in the paper were reproduced from the ASTER Spectral Library through the courtesy of the Jet Propulsion Laboratory, California Institute of Technology, Pasadena, California. Copyright © 1999, California Institute of Technology. ALL RIGHTS RESERVED. We thank Gabriel Senay, Limin Yang, Larry Tieszen, and three anonymous reviewers for providing valuable comments and suggestions.

References

Alsdorf, D.E., E. Rodríguez, and D.P. Lettenmaier, 2007. Measuring surface water from space, *Reviews of Geophysics*, 45:RG2002, doi:10.1029/2006RG000197.

Bryant, R.G., and M.P. Rainey, 2002. Investigation of flood inundation on playas within the Zone of Chotts, using a time-series of AVHRR, *Remote Sensing of Environment*, 2002(2–3):360–375.

California Institute of Technology – Jet Propulsion Laboratory, 2008. ASTER Spectral Library, URL: *http://speclib.jpl.nasa.gov/*, (last data accessed: 08 August 2009).

Chen, X., Y.S. Li, Z. Liu, K. Yin, Z. Li, O.W. Wai, and B. King, 2004. Integration of multi-source data for water quality classification in the Pearl River estuary and its adjacent coastal waters of Hong Kong, *Continental Shelf Research*, 2004(24):1827–1843.

Chipman, J.W., and T.M. Lillesand, 2007. Satellite-based assessment of the dynamics of new lakes in southern Egypt, *International Journal of Remote Sensing,* 28(19):4365–4379.

Gao B., 1996. NDWI – A normalized difference water index for remote sensing of vegetation liquid water from space, *Remote Sensing of Environment*, 58(3):257–266.

Hung, M.C., and Y.H. Wu, 2005. Mapping and visualizing the Great Salt Lake landscape dynamics using multi-temporal satellite images, 1972–1996, *International Journal of Remote Sensing,* 26(9):1815–1834.

Jain, S.K, R.D. Singh, M.K. Jain, and A.K. Lohani, 2005. Delineation of flood-prone areas using remote sensing technique, *Water Resources Management*, 19(4):337–347.

Jain, S.K., A.K. Saraf, A. Goswami, and T. Ahmad, 2006. Flood inundation mapping using NOAA AVHRR data, *Water Resources Management*, 20(6):949–959.

Lacaux, J.P., Y.M. Tourre, C. Vignolles, J.A. Ndione, and M. Lafaye, 2007. Classification of ponds from high-spatial resolution remote sensing: Application to Rift Valley Fever epidemics in Senegal, *Remote Sensing of Environment*, 106(1):66–74.

Li, J., and R.M. Narayanan, 2003. A shape-based approach to change detection of lakes using time series remote sensing images, *IEEE Transactions on Geoscience and Remote Sensing*, 41(11):2466–2477.

Lira, J., 2006. Segmentation and morphology of open water bodies from multispectral images, *International Journal of Remote Sensing,* 27(18):4015–4038.

Ma, M., X. Wang, F. Veroustraete, and L. Dong, 2007. Change in area of Ebinur Lake during the 1998–2005 period, *International Journal of Remote Sensing*, 28(24):5523–5533.

McFeeters, S.K., 1996. The use of Normalized Difference Water Index (NDWI) in the delineation of open water features, *International Journal of Remote Sensing*, 17(7):1425–1432.

Ouma, Y.O., and R. Tateishi, 2006. A water index for rapid mapping of shoreline changes of five East African Rift Valley lakes: An empirical analysis using Landsat TM and ETM+ data, *International Journal of Remote Sensing,* 27(15):3153–3181.

Rogers, A.S., and M.S. Kearney, 2004. Reducing signature variability in unmixing coastal marsh Thematic Mapper scenes using spectral indices, *International Journal of Remote Sensing*, 25(12):2317–2335.

Sakamoto, T, N.V. Nguyen, A. Kotera, H. Ohno, N. Ishitsuka, and M. Yokozawa, 2007. Detecting temporal changes in the extent of annual flooding within the Cambodia and the Vietnamese Mekong Delta from MODIS time-series imagery, *Remote Sensing of Environment*, 109(3):295–313.

Sethre, P.R., B.C. Rundquist, and P.E. Todhunter, 2005. Remote detection of prairie pothole ponds in the Devils Lake Basin, North Dakota, *GIScience and Remote Sensing*, 42(4):277–296.

Sippel, S.J., S.K. Hamilton, J.M. Melack, and B.J. Choudhury, 1994. Determination of inundation area in the Amazon River Floodplain using the SMMR 37 GHz polarization difference, *Remote Sensing of Environment*, 48(1):70–76.

Smith, L.C., 1997. Satellite remote sensing of river inundation area, stage, and discharge: A review, *Hydrological Processes*, 11(10):1427–1439.

Xu, H., 2006. Modification of normalised difference water index (NDWI) to enhance open water features in remotely sensed imagery, *International Journal of Remote Sensing*, 27(14):3025–3033.

(Received 25 September 2008; accepted 06 January 2009; revised 24 February 2009)